ARMA 21–1784

Viscoplastic modeling of elastic and creep deformation of fractured Berea sandstone

Talukdar, M. and Sone, H.
University of Wisconsin Madison, Madison, Wisconsin, USA
Griffith, W. A.
Ohio State University, Columbus, Ohio, USA

This paper was prepared for presentation at the 55th US Rock Mechanics/Geomechanics Symposium held in Houston, Texas, USA, 20-23 June 2021. This paper was selected for presentation at the symposium by an ARMA Technical Program Committee based on a technical and critical review of the paper by a minimum of two technical reviewers. The material, as presented, does not necessarily reflect any position of ARMA, its officers, or members. Electronic reproduction, distribution, or storage of any part of this paper for commercial purposes without the written consent of ARMA is prohibited. Permission to reproduce in print is restricted to an abstract of not more than 200 words; illustrations may not be copied. The abstract must contain conspicuous acknowledgement of where and by whom the paper was presented.

ABSTRACT: We observed and modeled the elastic, inelastic and time-dependent viscous properties of damaged Berea Sandstone samples to investigate the impact of damage on the rheological properties of rocks. Cylindrical Berea Sandstone plugs were prepared both parallel and perpendicular to bedding. We impacted the samples with Split Hopkinson Pressure Bar to pervasively fracture the specimens at different strain rates. Longitudinal mode-I fractures are dominant in specimens impacted at relatively low strain rates (about 130 /s), whereas shear fractures also form in specimens deformed at high strain rates (up to 250 /s). The damaged rocks were subjected to multiple steps of differential stress loading and hold stages under 15 MPa confining pressure. A key observation is that higher damaged specimens showed greater axial and volumetric creep strain deformation during loading and hold stages. Poisson ratio also increase with increasing damage. We modeled the volumetric strain of the sandstone specimens using a Perzyna viscoplasticity law that employs the Modified Cam Clay model as the yield criterion (Haghighat et al. 2020). We deduced that fractured rocks undergo substantial bulk time-dependent deformation due to volumetric compaction and fracture closure. Damage increase results in decrease of the effective viscosity of the material.

1. INTRODUCTION

Time-dependent compaction or loss of pore volume due to external applied stress is important to understand porosity loss in earth materials. Compaction is enhanced in semi to unconsolidated sediments due to the high pore volume in their structure. In field scale, compaction of unconsolidated sands in Wilmington field and San Joaquin valley, California has been reported to be a time-dependent process (Kosloff and Scott, 1980a). Similar observations have been proposed in Bolivar coast heavy oil fields (Schenk and Puig, 1983). Laboratory studies on dry, unconsolidated sandstone have shown considerable time-dependency in compaction of pore volume (Hagin and Zoback, 2004). These observations suggest that compaction and time-dependent deformation are closely related processes that determine the long-term behavior of porous materials.

Introduction of fractures in rocks increases the porosity due to the addition of fracture aperture volume to the volume of pores. Thus, we expect fractured rocks to also undergo considerable compaction in pore volume on application of force by both pore and fracture aperture closure, thereby enhancing viscous deformation in fractured rocks. The fracture planes may also act as slip planes which allow stable sliding along cracks, leading to bulk deformation of the material. This apparent ductile behavior of fractured rocks was studied in thermally fractured granite samples to show that time-dependent deformation is enhanced in samples with high fracture density (Sone and Condon, 2017).

Ductile deformation of fractured rocks may impact wells drilled in highly fractured areas of the crust. Field studies by Hennings et al. (2012) suggested that wells drilled in fractured zone are more productive in regions of high fracture density and in regions where fractures are critically oriented. Experimental measurement of permeability in damage rocks has shown permeability magnitude several degrees of magnitude higher than intact rocks (Lockner et al. 2000). While these studies suggest that fractures enhance permeability in fractured rocks, progressive compaction of the pore volume and sliding along cracks may reduce permeability at a higher rate than intact rocks. Therefore, studying ductile behavior of fractured rocks is critical to understand long term well performance.

Studying long term viscous properties of damaged rocks are also important to ensure long term safety and stability of underground storage caverns. Similarly, mechanical properties of fractured zones are essential parameters for mining design and roadway support. Current reservoir

simulation models also require bulk hydraulic properties of fractured systems, which is one of the greatest uncertainties in these models. There are limited in situ data of bulk properties of damage zones, therefore there is a need to constrain them experimentally. To address these issues, this study measures the bulk elastic and time-dependent properties of damaged materials under stress conditions resembling natural reservoirs.

First, we created pervasive fractures in Berea sandstone specimens by impacting samples at high strain rates. We conducted triaxial experiments on the fractured samples to observe the elastic, inelastic and time-dependent properties of damaged specimens. Deformation for these samples were characterized both parallel and perpendicular to bedding. Finally, to be able to fully characterize the elastic deformation and viscous compaction of damaged specimens at subsurface stress conditions, we used a viscoplastic model to simulate the experimental results.

2. METHODOLOGY

Split Hopkinson Pressure bar (SHPB) is used to dynamically impact specimens to study material properties under dynamic load. In an SHPB, a gas gun impacts a striker bar onto the incident bar. Higher the gas pressure, higher the velocity of the striker bar impacting the incident bar. The incident bar loads the sample placed between the incident and transmitted bar, leading to the propagation of stress waves. Strain gages are placed on the incident and transmitted bar of SHPB to calculate strain rate and stress using the theory of 1-D wave equation. On impacting samples with SHPB, strain localization in the rock specimen is hindered above certain strain rates. The primary reason to choose SHPB to impact Berea Sandstone specimen is to disrupt strain localization and foster pervasive damage throughout the specimen. Note that we have used the terms damage and fracture interchangeably in this article.

We acquired Berea Sandstone plugs from a block with a coring machine. The plugs were 1.5 inch (38.1 mm) in length and 1 inch (25.4 mm) in diameter. A length: diameter ratio was maintained at 3:2 instead of 2:1 (standard for triaxial tests) to reduce lateral expansion and bending of the core plugs on impact with the incident bar of SHPB. We dried all the specimens at 80º C for 12 hours in an oven under vacuum.

We placed metal disks, 0.2 inch (5 mm) in thickness and 1 inch (25.4 mm) in diameter on either ends of the plug for the SHPB tests. The metal disks were prepared of the same material (maraging steel) as the incident and transmitted bars of the SHPB to avoid impedance contrast between the bars and the metal. Subsequently, we jacketed the samples with polyolefin to retain the impacted rock inside the jacket during impact. We impacted the perpendicular/ vertical and parallel/ horizontal Berea Sandstone plugs at strain rates of 130-200 s^{-1} to create pervasive damage in the samples. Gas pressures of 15, 20 and 25 psi were maintained to create various degrees of damage. At low gas pressures, or low strain rates, we observed that most fractures created were longitudinal opening fractures, formed parallel to the direction of loading. However, at higher strain rates, the proportion of oblique shear fractures increase relative to the longitudinal opening fractures. We interpret that fewer

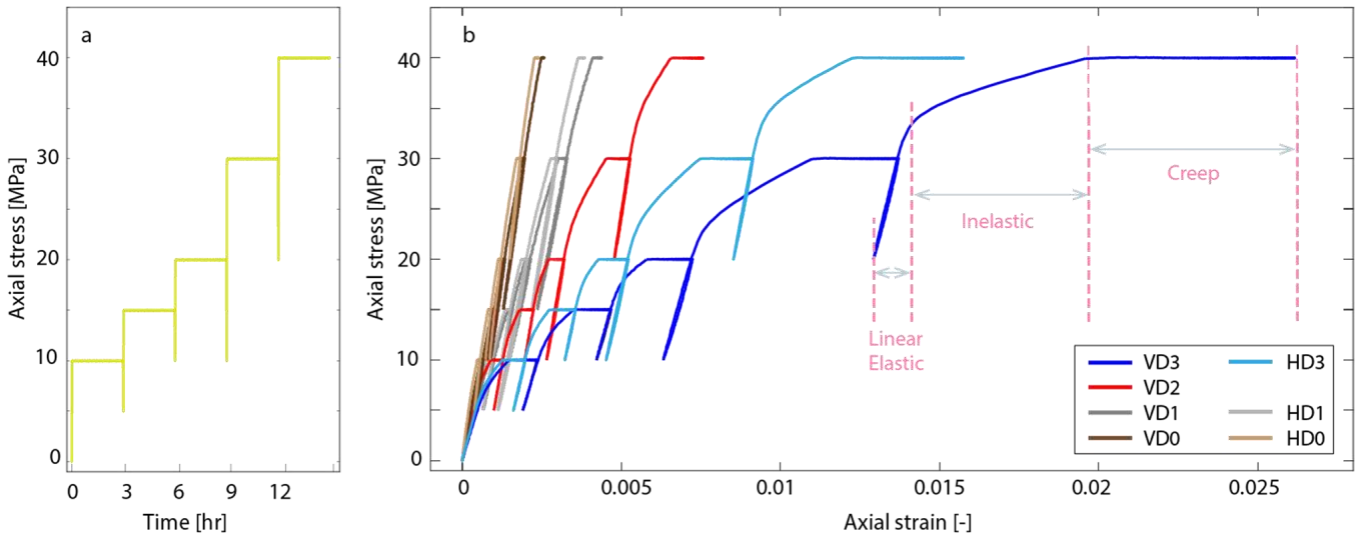

Fig. 1. a) Plot of stress input with time in the triaxial stage showing loading, unloading and hold/ creep stages. b) The axial strain response to the applied axial stress is plotted as stress-strain plots. Same colors indicate same damage intensities where lighter shades are samples loaded parallel to bedding (H) and darker shades represent samples loaded perpendicular to bedding (V). The plot shows how elastic, inelastic and creep deformation is higher for samples from left to right. The vertical samples deform more than the horizontal samples.

oblique fractures were created at low strain rates as the material expands laterally, whereas the rocks fail preferentially by shear as the rocks cannot expand laterally at higher strain rates. We note that this is somewhat analogous to the difference between a uniaxial stress boundary condition which allows lateral deformation and a uniaxial strain boundary condition which hinders lateral deformation.

The samples deformed at 15, 20 and 25 psi gas pressure are marked as D1, D2 and D3 respectively, designating increasing degree of damage. 'V' or 'H' in front of sample name indicates Vertical or Horizontal sample. We compared the damaged samples with an intact vertical (VD0) and horizontal sample (HD0).

We performed triaxial creep experiments at confining pressure of 5-15 MPa followed by axial differential stress of 10-40 MPa at 15 MPa confining pressure. We conducted the tests in room temperature and dry conditions (no pore fluid). During the hydrostatic stages, we applied confining pressure in steps of 5 MPa over 1 minute. After each step loading of hydrostatic pressure, we held hydrostatic stress constant for 3 hours to study hydrostatic creep response. Each hydrostatic creep stage is followed by confining pressure unloading and subsequent reloading. In the triaxial stage, we loaded the sample at axial differential stress of 10, 15, 20, 30 and 40 MPa and then held the axial stress constant for 3 hours at each stage to study triaxial creep at multiple axial loads. We only show the stress history of the triaxial stage in Figure 1a because we only discuss the results from the triaxial stage in this article.

We measured the output axial deformation response corresponding to the aforementioned input stress history with Linear Variable Differential Transducer (LVDT). We utilized strain gage-based sensors to record the lateral diameter change of the material. We attached two lateral sensors to characterize the anisotropy of the horizontal sample, i.e., we placed lateral sensors both parallel and perpendicular to the layer orientation. Although vertical samples are radially symmetric, we also attached two lateral sensors onto the vertical samples to take an average of the lateral deformation. We use measurements from both the lateral sensors to calculate bulk/ volumetric strain of the specimens. Out of the eight samples, we failed to accumulate feasible data for the horizontal sample damaged at 20 psi gas pressure (i.e., HD2). In the upcoming sections, we will present results for the seven samples we tested with our triaxial apparatus (three vertical damaged and one vertical intact sample, two horizontal damaged and one horizontal intact sample).

3. RESULTS

We compared the elastic and creep deformation of intact samples with that of damaged samples under triaxial conditions. Damaged samples showed higher axial deformation during the loading, creep and unloading stages than the intact sample (Fig. 1b). This phenomenon is observed in comparisons of VD3, VD2, VD1 with VD0 or HD3, HD1 with HD0. We also observed that more damage leads to greater elastic and creep deformation of the material. Failure planes within the more damaged specimens reduce the stiffness of the rock, leading to more axial elastic deformation in the rocks. Similar to previous observation which suggest that modulus correlate well with the tendency to creep in hold stage (Sone and Zoback, 2013), we observed more deformation in the hold stage for more fractured, less stiff rocks. More damaged rocks also showed more bulk/ volumetric strain.

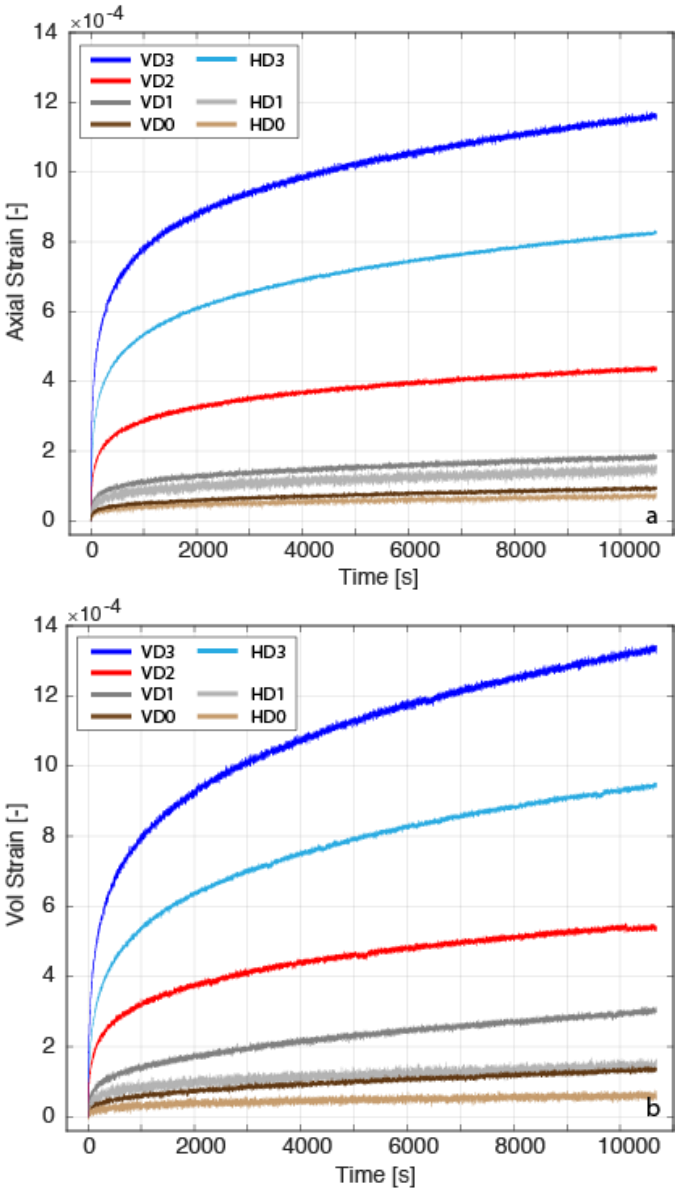

Fig. 2. Plots of a) axial and b) volumetric strain with time during the 15 MPa hold stage. Both curves show how creep strain increases with increasing damage. The vertical samples show more deformation than the horizontal samples.

From our experimental results, we observed that the intact vertical sample shows more elastic and creep deformation than the intact horizontal sample. Damaged rocks also show more axial and volumetric deformation in the vertical specimens than its horizontal counterparts (Fig. 2). A vertical sample is loaded perpendicular to the layers, also termed as an iso-stress condition. In an iso-stress condition, all the layers carry equal load, therefore the average stiffness is the harmonic average of each layer. Whereas, for a horizontal sample where the sample is loaded parallel to layers, the layers undergo same strain (iso-strain). The average stiffness of the rock in iso-strain condition is the arithmetic average. Mathematically, the harmonic average is always lower than the arithmetic average for positive numbers. Therefore, vertical stiffness is lower than horizontal. In other words, the vertical samples are expected to show more deformation than the horizontal counterparts (Sone and Zoback, 2013b; Trzeciak et al., 2018).

We also observed that the anisotropy is enhanced in the more damaged specimen, i.e., there is larger difference in axial strain for samples impacted at 25 MPa (difference between VD3 and HD3) than those impacted at 15 MPa (difference between VD1 and HD1) as shown in Figure 2a,b. We attribute this behavior to preferential alignment of fractures along the layers for horizontal samples, which enhanced the anisotropy between the vertical and horizontal samples.

Previous studies have suggested that with increase in damage, Poisson ratio increase (Faulkner et al., 2006; Pimienta et al., 2018). Similarly, we observed that the Poisson ratio is higher for samples with higher damage (Fig. 3). Poisson ratio is also seen to increase at high differential stress.

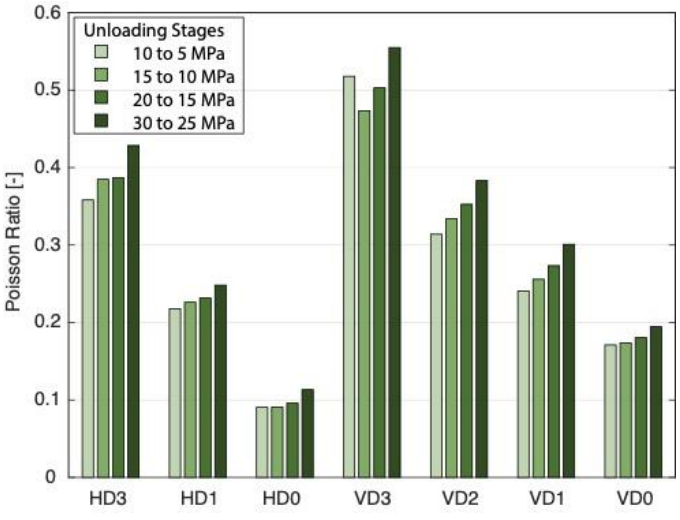

Fig. 3. Poisson ratio calculated from the unloading stages after each creep stage, because the unloading stage is representative of elastic deformation. Darker shades are for higher differential stress magnitudes.

4. VISCOPLASTIC CONSTITUTIVE LAW

Various constitutive relations have been proposed to understand the time-dependent properties of rocks. While some studies suggest a power law relationship to characterize creep deformation (Sone and Zoback, 2013b), other studies have used Prony series (Trzeciak et al. 2017). Both power law and Prony series are time functional forms. Power law models are suited for models where the time duration of interest is long. On the other hand, for Prony series, the retardation times are difficult to constrain. Other rheological models like Maxwell, Fractional Maxwell, Kelvin and Burgers models have been used to fit creep data (Xing et al. 2017). Nonetheless, these models are also time functional forms, therefore, they are not able to capture anelastic behavior seen between the loading and unloading stages. This highlights the need for a model without time functional form (Haghighat et al. 2020). We use the constitutive law developed by Haghighat et al. (2020) to constrain creep parameters from our experimental data. Unlike the earlier mentioned time functional rheological models, this model utilizes only stress path as an input to predict the resultant elastic and plastic strain during deformation.

The model by Haghighat (2020) uses a combination of Modified Cam Clay model and Perzyna viscoplastcity (Perzyna, 1966) to constrain parameters from the experimental data. Modified Cam clay model is an elasto-plastic strain hardening model that captures the essential aspects of soil behavior: strength, dilatancy, compression and critical state. In the critical state of a material, the material can undergo distortion without any changes in stress or volume. In the pressure-deviatoric stress plane, the critical state line is a straight line which passes through the origin and has a characteristic slope η, η being a material property. Physically, the critical state line is the boundary that separates brittle localized failure from distributed deformation. The value of η is one of the main parameters in the definition of the yield surface. The value η is comparable to friction in rock mechanics experiments and there exists a relationship between η and Mohr-Coulomb frictional angle ϑ (Zoback, 2010).

$$\eta = \frac{6 \sin \vartheta}{3 - \sin \vartheta} \quad (1)$$

We use the Modified Cam Clay (MCC) yield criterion to delineate the elastic and plastic part of the deformation. The MCC yield surface is an ellipse in the pressure p-deviatoric stress q space. The size of the yield surface is dependent on whether the material is undergoing strain hardening or strain softening (Schofield and Wroth, 1968). Strain hardening is when an increasing stress is required for additional plastic deformation to accumulate whereas during strain softening, there is decrease of stress with increase in strain. When the material is compacted

by increasing stress as in strain hardening, the MCC yield envelope increases in size, i.e., even more stress is required for a compacted material to reach the yield envelope. The yield envelope which expands or shrinks in the p-q space can be written mathematically as:

$$F = \frac{q^2}{\eta^2} + p(p - p_y) \tag{2}$$

Where F is the yield function and p_y is the yield stress. When the yield function is zero, the elliptical yield envelope neither expands nor contracts.

Pore volume change is another important aspect of this model. One way to quantify pore volume in porous and low cohesion materials is the use of void ratio (e), which is the ratio of pore volume and material volume. During soil mechanics experiments of compression and swelling, it is observed that void ratio has a linear relationship with logarithm of the pressure during loading and unloading (Wood, 1990). Since loading involves both elastic and plastic deformation, the slope of the straight line in void ratio- log pressure plot is different than that of the slope of the unloading line in the void ratio-log pressure plot where deformation is elastic. The loading line and unloading lines in the void ratio-log pressure space is widely known in the soil mechanics literature as isotropic compression line and swelling line, respectively, given by:

$$de = -\lambda\, d(\ln p) \tag{3}$$

$$de^e = -\kappa\, d(\ln p) \tag{4}$$

Where e is the void ratio and e^e is the elastic portion of void ratio. The loading and unloading slopes are denoted as λ and κ, respectively. We can use Eq. 3 and 4 to write yield stress as a function of volumetric plastic strain (ε_v^p), λ and κ if we assume that the total strain is a sum of the elastic and plastic component of strain.

$$p_y = p_{y0} \exp\left(\frac{1+e_0}{\lambda-\kappa}\, \varepsilon_v^p\right) \tag{5}$$

Where p_{y0} and e_0 pre-consolidation stress and initial void ratio, respectively. The elastic response of the material is described by combining the equation for swelling line (Eq. 4) with the definition of strain in large deformation in terms of deformation gradient. To express the non-linear elastic part of the deformation, pressure dependent bulk modulus is expressed in terms of void ratio and κ.

$$K = \frac{1+e}{\kappa} p \tag{6}$$

An energy-based definition of strain hardening, and softening was proposed by Drucker, also called the Drucker Inequality (Drucker, 1950). The Drucker Inequality states that for a single stress component, the conjugate plastic strain rate satisfies $\dot{\sigma}\dot{\varepsilon^p} \geq 0$ for work hardening material. The inequality is unchanged if the stress and strain rates are multiplied by an infinitesimal time to get the same forms as $d\sigma d\varepsilon^p \geq 0$ for work hardening material. This product has the dimensions of work per unit volume. Since elastic component of strain can never be zero or negative for work hardening materials, we can write the work hardening equations as $d\sigma d\varepsilon > 0$ and $d\sigma d\varepsilon^p \geq 0$. These two inequalities also work for perfectly plastic material where $d\sigma = 0$. They become $d\sigma d\varepsilon^p = 0$; but $d\sigma d\varepsilon > 0$. For work softening materials, since $d\sigma < 0$, and $d\varepsilon^p < 0$; $d\sigma d\varepsilon^p \geq 0$ holds. This common inequality $d\sigma d\varepsilon^p \geq 0$ for work hardening, work softening, and perfectly plastic materials suggest that the work done due to plastic deformation is always non-negative, also the basis for the postulate of maximum plastic dissipation (Simo and Hughes, 2006). Solving the principle of maximum plastic dissipation for viscosity (μ) based Perzyna formulation, the equation for plastic strain rate is obtained.

$$\dot{\varepsilon_v^p} = \frac{1}{\mu}\frac{1}{p}\left(\frac{q^2}{\eta^2} + p\big(p - p_y\big)\right)(2p - p_y) \tag{7}$$

Where $\frac{1}{p}\left(\frac{q^2}{\eta^2} + p\big(p - p_y\big)\right)(2p - p_y)$ is overstress and μ is viscosity.

Viscosity μ is the only unknown parameter in the above formulation. Here we assume viscosity as an exponential function of volumetric plastic strain (Haghighat et al. 2020).

$$\mu = \mu_0 \exp(\zeta\, \varepsilon_v^p) \tag{8}$$

Where μ_0 and ζ are material constants.

5. DISCUSSION

We use the above formulation by Haghighat et al. (2020) to characterize the viscoplastic rheology of damage zones. Our objective is also to compare the rheology of damage and intact rocks to discuss how the plastic strain rate and overstress evolves during time-dependent deformation. We calculate plastic strain rate at each step using Eq. 7 from viscosity, approximated from Eq. 8. Then, we use a finite difference approximation to calculate plastic strain at each step from plastic strain rate. The values of $p_{y0}, \lambda, \kappa, \mu_0, \zeta, e_0$ and η can be varied to get different plastic strain and plastic strain rate magnitudes.

We constrained the value of initial void ratio e_0 in Eq. 5 from the initial porosity of Berea Sandstone. Porosity of the samples is measured with a helium porosimeter before impacting the samples with SHPB. The mean porosity of the rock, measured with porosimeter was found to be

20%, which corresponds to a void ratio of e_0=0.25 (since $e = \phi/(1-\phi)$). We calculate fracture porosity created by impacting the sample with SHPB by measuring the volume of the sample before and after impact. The difference of volume before and after impact, in other words, fracture porosity is added to sample porosity to calculate initial void ratio (e_0) (Table 1). Apart from constraining e_0, we also constrained η by assuming the coefficient of internal friction to be 0.6 for all the samples (Eq. 1).

Table 1. Calculating void ratio from sample dimensions.

#	Gas Pres [psi]	Initial Volume [mm^3]	Final Volume [mm^3]	Porosity Change [%]	Void Ratio
HD3	25.1	19593.56	21117.39	7.777	0.385
HD1	15.3	19079.01	29342.96	6.625	0.363
HD0	0	19827.11	19827.11	0	0.250
VD3	24.9	19751.57	21285.61	7.767	0.384
VD2	20.6	19790.06	21279.14	7.524	0.379
VD1	15.3	20370.46	21250.22	4.319	0.321
VD0	0	19467.89	19467.89	0	0.250

We assign initial values of the rest of the five variables: p_{y0}, λ, κ, μ_0 and ζ for finite difference modeling, followed by optimization to solve for the parameters that best simulates the experimental results. The formulation for plastic strain rate in Eq. 7 fits the experimental volumetric strain-time plot but fails to fit the stress-strain plot (Talukdar et al. 2020). Therefore, we introduce an exponent N to the overstress term to be able to produce higher plastic strain rate during the loading stages so as to fit the stress-strain data.

$$\dot{\varepsilon}_v^p = \frac{1}{\mu}\left[\frac{1}{p}\left(\frac{q^2}{\eta^2} + p(p-p_y)\right)(2p-p_y)\right]^N \quad (9)$$

Introducing the exponent N changes the unit of viscosity from [MPa. s] to [MPa ^{N}. s].

In Table 2, we present a compilation of the optimized parameters for the horizontal and vertical Berea Sandstone specimens. We observe that with increasing damage, λ and κ increases. This is because for the same pressure change, the change in void ratio is higher for more damaged specimens as compared to less damaged specimens. A clear correlation of p_{y0} with damage is not

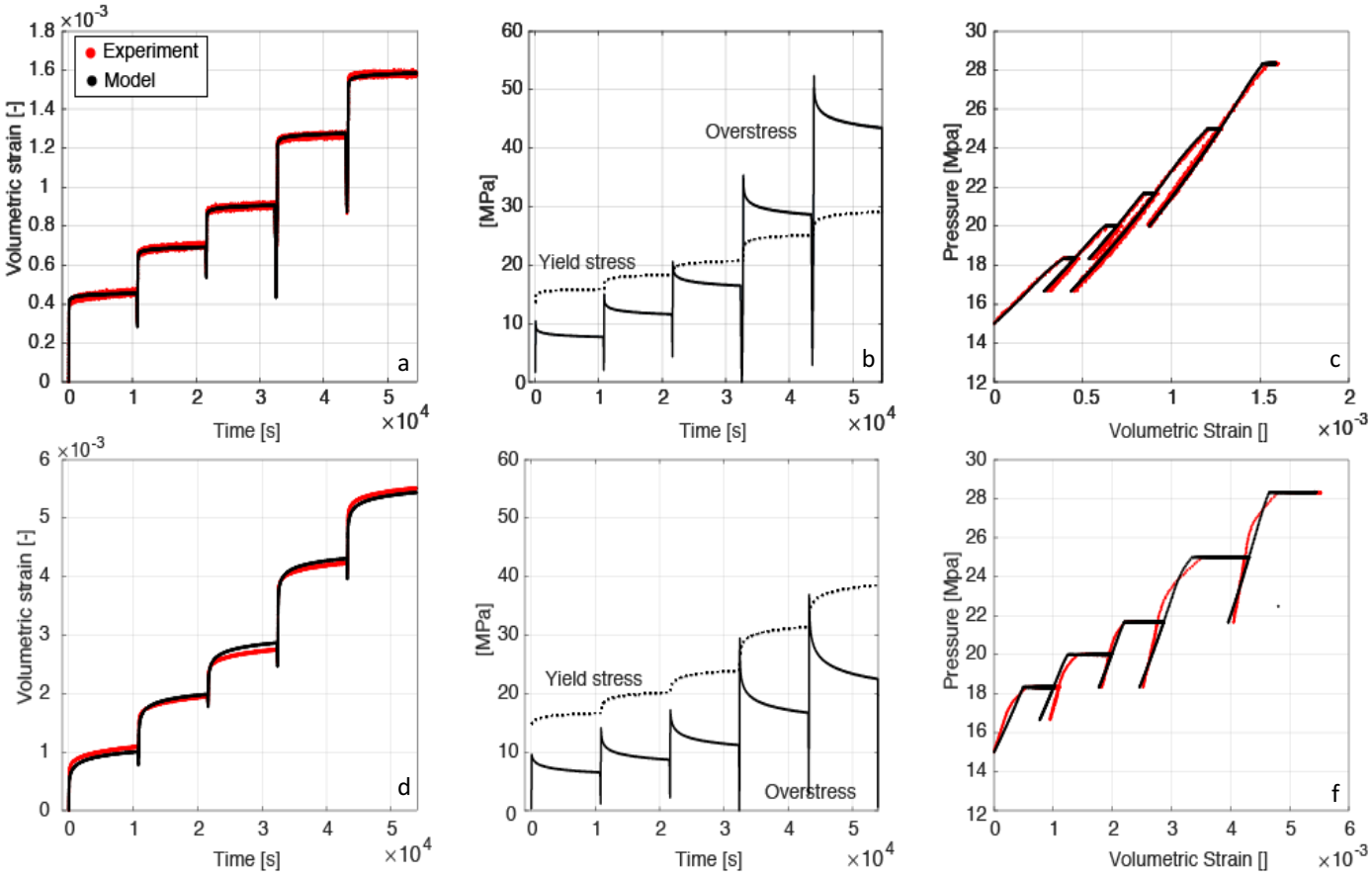

Fig. 4. a) Experimental and simulated Volumetric strain-Time plot for intact vertical sample VD0. b) Yield stress and overstress evolution with time for VD0. c) Experimental and simulated Pressure-Volumetric Strain plot for VD0. 4. d,e,f) Similar plots for a damaged vertical sample VD2 for comparison. Y-axis labels for 4.a and 4.d shows that VD0 undergoes less creep deformation than VD2. In 4.e, higher creep strain in VD2 is fitted with large changes in overstress during the hold stages as compared to VD0 in 4.b. Plastic strain rate or rate of viscous deformation is amplified for the damaged sample as compared to the intact sample, leading to faster decrease in overstress in the damaged specimen VD2.

found in the samples, whereas we observe a decrease in μ_0, ζ and N with increase in damage.

Table 2. Optimized parameters to fit the experimental data

#	λ (10^{-3})	κ (10^{-3})	p_{y0}	μ_0	ζ	N
HD3	8.83	2.33	17.15	1.2 e8	0.46	3.9
HD1	7.36	1.22	15.50	2.8 e9	1.1e3	5.8
HD0	1.83	1.15	14.78	5.5e15	6.6e3	14.5
VD3	7.50	2.44	14.71	1.2e14	3.0e3	8.3
VD2	4.90	2.21	13.34	4.4e14	5.8e3	8.1
VD1	2.26	1.37	15.01	1.8e12	11e3	5.1
VD0	2.53	1.20	13.54	1.5e18	64e3	13.1

Two examples of simulation fitting are shown in Fig. 4. We present our solutions for an undamaged vertical sample VD0 (Fig. 4.a, 4.b, 4.c) and a damaged vertical sample VD2 (Fig. 4.d, 4.e, 4.f). We observe that the overstress achieved in the intact sample is higher than the overstress achieved by the damaged sample (Fig. 4.b, 4.e). Overstress diminishes faster in the creep stages of the damage sample. This deceleration of overstress in the creep stage of the damaged sample as compared to the intact sample signify more viscous deformation in damaged rocks due to high plastic strain rate in damaged rocks. Increase in plastic strain rate $\dot{\varepsilon}_v^p$ in the damage sample corresponds to a decrease in effective viscosity μ in damaged samples, as in Eq. 7 or 9. Decrease in μ_0 and N with damage in Table 2 reflects the plastic strain rate increase with damage.

6. CONCLUSION

We have shown with laboratory experiments that elastic, inelastic and creep strain is significantly enhanced in fractured rocks as compared to intact rocks. More fractured samples exhibited more deformation. Samples with different layer orientation but impacted at same gas pressures showed less deformation parallel to bedding deformed than perpendicular to bedding. The variability in observations due to damage and sample anisotropy underlines the importance of considering these factors in material characterization.

The fracture volume introduced with SHPB was compacted at low to high differential stress magnitudes to quantify plastic strain rate, viscosity and overstress of damaged rocks using a viscoplastic model. From our simulation results, we observed larger drops in overstress during the creep stages for the damage sample as compared to intact rocks. Larger drop is overstress in samples with more fracture porosity is attributed to higher plastic strain rate or higher rate of viscous compaction, but lower effective viscosity of damaged rocks. However, a direct correlation between viscosity changes and pore volume reduction still remains unexplored. Quantitative analysis on how these parameters correlate can provide more insights into how fracture volume evolves over time and in turn control long term behavior of fractured rock masses.

REFERENCES

1. Ding, X., G. Zhang, B. Zhao and Y. Wang. 2017. Unexpected viscoelastic deformation of tight sandstone: Insights and predictions from the fractional Maxwell model. *Scientific reports*, 7(1), pp.1-11.

2. Drucker, D.C., 1950. Some implications of work hardening and ideal plasticity. *Quarterly of Applied Mathematics*, 7(4), pp.411-418

3. Faulkner, D.R., T.M. Mitchell, D. Healy and M.J. Heap. 2006. Slip on 'weak' faults by the rotation of regional stress in the fracture damage zone. *Nature*, 444 (7121), pp.922-925.

4. Haghighat, E., F.S. Rassouli, M.D. Zoback and R. Juanes. 2020. A viscoplastic model of creep in shale. *Geophysics*, 85(3), pp.MR155-MR166.

5. Hagin, P.N. and M.D. Zoback. 2004. Viscous deformation of unconsolidated reservoir sands—Part 1: Time-dependent deformation, frequency dispersion, and attenuation. *Geophysics*, 69(3), pp.731-741.

6. Hennings, P., P. Allwardt, P. Paul, C. Zahm, R. Reid, H. Alley, R. Kirschner, B. Lee and E. Hough. 2012. Relationship between fractures, fault zones, stress, and reservoir productivity in the Suban gas field, Sumatra, IndonesiaSuban Gas Field, Sumatra, Indonesia. *AAPG bulletin*, 96(4), pp.753-772.

7. Kosloff, D., R.F. Scott and J. Scranton. 1980. Finite element simulation of Wilmington oil field subsidence: Linear modelling. *Tectonophysics*, 65(3-4), pp.339-368.

8. Lockner, D., H. Naka, H. Tanaka, H. Ito and R. Ikeda. 2000. Permeability and strength of core samples from the Nojima fault of the 1995 Kobe earthquake. *Proceedings of the international workshop on the Nojima fault core and borehole data analysis*. Vol. 129, pp. 147-152. Tsukuba, Japan: US Geol. Sur.

9. Perzyna, P., 1966. Fundamental problems in viscoplasticity. *Advances in Applied mechanics*. Vol. 9, pp. 243-377. Elsevier.

10. Pimienta, L., A. Schubnel, M. Violay, J. Fortin, Y. Guéguen, and H. Lyon-Caen. 2018. Anomalous Vp/Vs ratios at seismic frequencies might evidence highly damaged rocks in subduction zones. *Geophysical Research Letters,* 45(22), pp.12-210.

11. Schenk, L. and F. Puig. 1982, November. Aspects of Compaction/Subsidence in the Bolivar Coast heavy oil fields highlighted by performance data of the M-6 project

area. *Proceedings of 1982 Forum on Subsidence due to Fluid Withdrawals* (pp. 109-120)

12. Schofield, A.N. and P. Wroth. 1968. Critical state soil mechanics (Vol. 310). London: *McGraw-hill.*

13. Simo, J.C. and T.J. Hughes. 2006. Computational inelasticity (Vol. 7). *Springer Science & Business Media*

14. Sone, H. and K.J. Condon. 2017, August. Ductile behavior of thermally fractured granite rocks. In *51st US Rock Mechanics/Geomechanics Symposium. American Rock Mechanics Association.*

15. Sone, H. and M.D. Zoback. 2013. Mechanical properties of shale-gas reservoir rocks—Part 2: Ductile creep, brittle strength, and their relation to the elastic modulus. *Geophysics*, 78(5), pp. D393-D402.

16. Sone, H. and M.D. Zoback 2014. Time-dependent deformation of shale gas reservoir rocks and its long-term effect on the in-situ state of stress. *International Journal of Rock Mechanics and Mining Sciences*, 69, pp.120-132.

17. Talukdar, M., H. Sone, W.A. Griffith and M.J. Braunagel. 2020, December. Creep deformation of synthetic damage zone rocks created from Split Hopkinson Pressure Bar tests. In *AGU Fall Meeting 2020*. AGU.

18. Trzeciak, M., H. Sone and M. Dabrowski. 2018. Long-term creep tests and viscoelastic constitutive modeling of lower Paleozoic shales from the Baltic Basin, N Poland. *International Journal of Rock Mechanics and Mining Sciences*, 112, pp.139-157.

19. Trzeciak, M., H. Sone and M. Dabrowski. 2017, August. Shale Creep Data Extrapolation: Comparing Different Data Fitting Methods and Its Uncertainties. In *51st US Rock Mechanics/Geomechanics Symposium. American Rock Mechanics Association.*

20. Wood, D.M., 1990. Soil behaviour and critical state soil mechanics. *Cambridge university press*

21. Zoback, M.D., 2010. Reservoir geomechanics. *Cambridge University Press*.